PNAS INAUGURAL ARTICLE | CELL BIOLOGY

cAMP/PKA signaling regulates TDP-43 aggregation and mislocalization

Diana M. Ho[a], Muhammad Shaban[b,c,d,e], Faisal Mahmood[b,c,d,e], Payel Ganguly[a], Leonardo Todeschini[a,1], David Van Vactor[a,2], and Spyros Artavanis-Tsakonas[a,2,3]

This contribution is part of the special series of Inaugural Articles by members of the National Academy of Sciences elected in 2023.
Contributed by Spyros Artavanis-Tsakonas; received January 12, 2024; accepted May 3, 2024; reviewed by Nancy M. Bonini and Arthur L. Horwich

Cytoplasmic mislocalization and aggregation of TDP-43 protein are hallmarks of amyotrophic lateral sclerosis (ALS) and are observed in the vast majority of both familial and sporadic cases. How these two interconnected processes are regulated on a molecular level, however, remains enigmatic. Genome-wide screens for modifiers of the ALS-associated genes *TDP-43* and *FUS* have identified the phospholipase D (Pld) pathway as a key regulator of ALS-related phenotypes in the fruit fly *Drosophila melanogaster* [M. W. Kankel *et al.*, Genetics 215, 747–766 (2020)]. Here, we report the results of our search for downstream targets of the enzymatic product of Pld, phosphatidic acid. We identify two conserved negative regulators of the cAMP/PKA signaling pathway, the phosphodiesterase *dunce* and the inhibitory subunit *PKA-R2*, as modifiers of pathogenic phenotypes resulting from overexpression of the *Drosophila TDP-43* ortholog *TBPH*. We show that knockdown of either of these genes results in a mitigation of both TBPH aggregation and mislocalization in larval motor neuron cell bodies, as well as an amelioration of adult-onset motor defects and shortened lifespan induced by TBPH. We determine that PKA kinase activity is downstream of both TBPH and Pld and that overexpression of the PKA target CrebA can rescue TBPH mislocalization. These findings suggest a model whereby increasing cAMP/PKA signaling can ameliorate the molecular and functional effects of pathological TDP-43.

ALS | TDP-43 | cAMP/PKA signaling | proteinopathy | neurodegeneration

Significance

Amyotrophic lateral sclerosis (ALS) is a devastating and fatal neurodegenerative disease with no known cure. Aggregation and cytoplasmic mislocalization of Transactive Response DNA binding protein of 43 kD (TDP-43) are hallmarks of ALS and likely have critical causative consequences for disease progression. The cellular factors that can regulate these processes hold promise as therapeutic targets but are still largely unknown. Using a genetic approach in *Drosophila*, we find that the neurologically significant cyclic AMP (cAMP)/Protein Kinase A (PKA) signaling pathway regulates the subcellular localization, aggregation, and function of TDP-43, thus raising the possibility that stimulation of this pathway may have beneficial effects on TDP-43 pathology in ALS.

Amyotrophic lateral sclerosis (ALS), also known as Lou Gehrig's disease, is a catastrophic and currently incurable disorder characterized by rapid progressive degeneration of motor neurons in the brain and spinal cord resulting in muscle weakness, atrophy, and inevitably death (1). Familially inherited ALS (fALS), which comprises ~10% of known cases, has been associated with mutations in over 20 genes (2). Among these is *Transactive Response DNA binding protein of 43 kD (TDP-43)*, which is mutated in a small minority (~3%) of fALS cases (3–5). In contrast, the underlying causes and risk factors for sporadic ALS (sALS; ~90% of cases) are poorly understood and likely to reflect a diverse and complex combination of genetic and environmental inputs (1, 6).

Notwithstanding the underlying genetic complexity, certain common pathological elements have emerged as hallmarks of ALS (7). Perhaps the most striking of these is the presence of TDP-43 protein aggregates in affected motor neurons; such inclusions are observed in ~97% of all ALS patients regardless of TDP-43 mutational status or whether the disease is familial or sporadic (8–10). Abnormal accumulation of TDP-43 is also a common occurrence in several other neurodegenerative disorders, including frontotemporal dementia, Parkinson's Disease (PD), and Alzheimer's Disease (AD) (9, 11).

TDP-43 aggregate pathology in the disease state is generally accompanied by changes in the relative levels of TDP-43 protein in the nucleus vs. the cytoplasm, a homeostatic imbalance that has both gain- and loss-of-function consequences (10, 12). There is strong evidence that these cellular processes are intimately associated with ALS-related functional neurodegeneration; moreover, they are likely to be coregulated (10, 12). Understanding the underlying mechanisms and genetic factors that regulate subcellular localization and aggregation of TDP-43 is thus of great importance to the development of effective therapeutics for ALS and other TDP-43-related proteinopathies.

The relative rarity of mutations in TDP-43 itself compared to the near-ubiquity of TDP-43 pathology in ALS (3) suggests that changes in the regulatory architecture surrounding TDP-43 are likely to be of paramount importance. In the current study, we use the fruit fly *Drosophila melanogaster* to dissect the genetic and cellular parameters that influence the subcellular behavior of the highly conserved fly *TDP-43* ortholog, *TBPH*. A large body of work has

Reviewers: N.M.B., University of Pennsylvania; and A.L.H., Yale University School of Medicine.

The authors declare no competing interest.

[1]Present address: Department of Cellular, Computational and Integrative Biology, University of Trento, Trento 38123, Italy.

[2]D.V.V. and S.A.-T. contributed equally to this work.

[3]To whom correspondence may be addressed. Email: artavanis@hms.harvard.edu.

This article contains supporting information online at https://www.pnas.org/lookup/suppl/doi:10.1073/pnas.2400732121/-/DCSupplemental.

Published June 5, 2024.

established *Drosophila* as a valuable model to study ALS and other neurodegenerative disorders (2, 13). Notably, the majority of ALS-relevant genes are conserved, and human TDP-43 and fly TBPH both induce ALS-like phenotypes including toxicity, neurodegeneration, and motor defects when overexpressed in flies (14, 15). We previously leveraged the powerful genetic tractability of this model to systematically screen for genetic modifiers of neurodegenerative phenotypes associated with misexpression of mutant TDP-43 and another gene mutated in fALS, *Fused in Sarcoma* (*FUS*) (16). We thus identified numerous modifier genes, including Phospholipase D (Pld/PLD), a key source of the pleiotropic lipid second messenger phosphatidic acid (PA), and several of the upstream regulators of the Pld pathway (16).

Here, we pinpoint the conserved phosphodiesterase *dunce/PDE4* and the PKA negative regulatory subunit *PKA-R2* as downstream components of the TDP-43/Pld/PA signaling axis and present evidence suggesting that cAMP/PKA signaling activity may play an important and unappreciated role in regulating TDP-43 localization and aggregation in ALS.

Results

Identification of dnc and PKA-R2 as Potential TBPH Modifiers. Mutations in the genes *TDP-43* and *FUS* have been identified as causative factors for ALS (17). Previously, we identified phospholipase D (Pld) and five upstream components of the Pld pathway as part of the underlying genetic architecture regulating TDP-43 and FUS in *Drosophila* ALS models (16). Pld catalyzes the conversion of phosphatidylcholine to PA, a pleiotropic molecule that feeds into multiple downstream signaling pathways to affect diverse processes in the cell (18, 19). The means by which PA subsequently impacts the downstream phenotypic effects of TDP-43 and FUS, however, remained unclear.

In order to identify modifiers that might act downstream of Pld/PA to affect ALS phenotypes, we cross-referenced the entire list of 696 TDP-43 and FUS modifiers from our earlier genome-wide screens (16) with a list of 50 genes (corresponding to 100 *Drosophila* orthologs) previously reported to interact directly with PA (20). We thus identified 12 overlapping genes that are both ALS modifiers and PA interactors (Fig. 1*A*). One of these genes is *dunce (dnc)*, the *Drosophila* ortholog of the mammalian Phosphodiesterase 4 (*PDE4*) genes. PA has been reported to bind directly to PDE4A and PDE4D in mammalian cells (21, 22). *Dnc/PDE4* catalyzes the hydrolysis of cAMP into GMP and AMP, and thus functions as a negative regulator of the core cAMP/PKA signaling pathway, which has been well established as a regulator of neuronal excitation, neural plasticity, and learning/memory via studies in *Drosophila* and other systems (23–26). Two additional members of the cAMP/PKA pathway, *Protein kinase, cAMP-dependent, regulatory subunit type 2* (*PKA-R2*, human ortholog: *PRKAR2A*) and *Exchange protein directly activated by cAMP* (*EPAC*, human ortholog: *RAPGEF4*) are also present in our list of TDP-43/FUS modifiers but were not previously reported to be PA interactors (Fig. 1*A*). Notably, *PKA-R2*, like dnc, is also a negative regulator of cAMP/PKA signaling (27).

We first validated this observation by testing RNAi lines against *dnc* and *PKA-R2* in our original screening model, where overexpression of the human disease-associated $hTDP\text{-}43^{M337V}$ allele in the fly eye using the *GMR-Gal4* driver causes a retinal degeneration phenotype characterized by loss of pigmentation and disrupted ommatidial structure that can be altered by perturbation of modifier genes (16). Both *dnc RNAi* and *PKA-R2 RNAi* were able to suppress this degenerative phenotype, with *PKA-R2 RNAi* effecting a qualitatively stronger rescue (*SI Appendix*, Fig. S1 *A–D*).

To further corroborate that *dnc* and *PKA-R2* are bona fide *TDP-43* modifiers, we asked whether knockdown of either gene via RNAi could affect two independent TDP-43-associated phenotypes, toxicity and adult lifespan reduction. In our previous study, we generated transgenic fly lines carrying either wild-type *UAS-TBPH* or *UAS-TBPH* bearing the *N493D* mutation, a cognate for the fALS-associated human *N378D* mutation (16). When either of these lines is driven by the eye-specific *GMR-Gal4* driver, we observe a high degree of pupal lethality, with *GMR-Gal4/CyO; UAS-*$TBPH^{N493D}$*/TM6b,* Tb^{1}*, TubP-Gal80* x w^{1118} crosses producing no adult nonbalancer progeny (i.e., 100% lethality) and *GMR-Gal4/CyO; UAS-*$TBPH^{WT}$*/TM6b,* Tb^{1}*, TubP-Gal80* x w^{1118} producing only rare escapers (comprising only 1% of total progeny, vs. an expected Mendelian ratio of 25%) (Fig. 1*B*). This is consistent with our previous study, where we found that $TBPH^{N493D}$ and $TBPH^{WT}$ generally induced similar phenotypes, with $TBPH^{N493D}$ often being somewhat stronger (16). Inhibition of either *dnc* or *PKA-R2* (*UAS-dnc RNAi* or *UAS-PKA-R2 RNAi*) in this background strongly increased the number of live adult nonbalancer progeny to near-Mendelian ratios for both $TBPH^{N493D}$ (22% and 25%, respectively) and $TBPH^{WT}$ (27% and 29%, respectively) and correspondingly decreased the number of pupal lethal individuals (Fig. 1*B*), indicating that reduction of either *dnc* or *PKA-R2* function can reduce TBPH-induced lethality. Neither of the RNAi lines alone caused significant lethality (Fig. 1*B*).

Simultaneously, we examined whether *dnc RNAi* or *PKA-R2 RNAi* could rescue TBPH-induced reduction of adult lifespan. We used the motor neuron-specific *OK371-Gal4* driver in combination with the temperature-sensitive *gal80.ts* allele to restrict transgene expression to adults (28), thereby eliminating any potential developmental effects. When a wild-type Flag-tagged TBPH (*UAS-TBPH-Flag*) is overexpressed in this background, the mean lifespan of adult flies decreases by ~50% compared to WT controls (22 d for *TBPH-Flag* vs. 44 d for controls, $P < 0.001$) (Fig. 1*C*). This severe reduction of lifespan is significantly rescued by *Pld RNAi* (mean 34 d, $P < 0.001$), *dnc RNAi* (mean 32 d, $P < 0.001$), or *PKA-R2* RNAi (mean 34 d, $P < 0.001$) (Fig. 1*C*). Similarly, lifespan reduction induced by adult-onset expression of the human $TDP\text{-}43^{M337V}$ allele with the motor neuron–specific *OK6-Gal4* driver is also partially mitigated by *dnc RNAi* (*SI Appendix*, Fig. S1*E*). These data indicate that *dnc* and *PKA-R2* are bona fide modifiers of TBPH phenotypes in multiple, independent models utilizing both fly and human TDP-43.

Pld/PKA Pathway Components Reduce TBPH Aggregation in a Motor Neuron-Based Aggregation Model. Aggregation of ectopic TDP-43 in the cytoplasm of affected cells is one of the hallmarks of ALS and is often associated with disease progression (7). We established a motor neuron-based TBPH aggregation model by overexpressing high levels of *UAS-*$TBPH^{WT}$ using the *Dip-α-Gal4* driver, which is active in a small, easily identifiable subset of motor neurons in the larval ventral nerve cord (VNC) (29). TBPH protein formed large cytoplasmic aggregates in the MNISN-IS cell, as visualized by immunostaining with an α-TBPH antibody (Fig. 2*A*). The N493D mutation did not appear to affect the degree of aggregation in this assay (*SI Appendix*, Fig. S2 *A* and *B*). Knockdown of *Pld* in this background led to a noticeable change in the appearance of the cytoplasmic aggregates, which become smaller and more numerous (Fig. 2*B*). Even more strikingly, knockdown of either *dnc* (Fig. 2*C*) or *PKA-R2* (Fig. 2*D*) resulted in a much more diffuse, but still granular, distribution of TBPH throughout the cytoplasm.

We scored the degree of aggregation in single T3 MNISN-IS cells using both qualitative and quantitative scales. For the former, we assigned each cell a relative score of 1 (least aggregated) to 4 (most aggregated) based on visual inspection. More than half of the cells

A

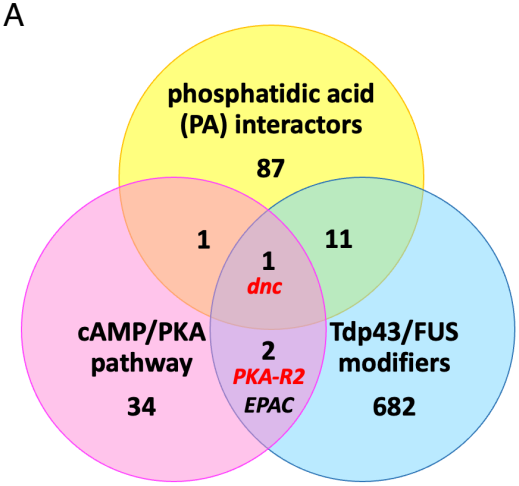

B

CRCSS GENOTYPE	non-bal progeny	total progeny	Obs ratio	expected mendelian ratio	Pupal lethal (non-Tb)
GMR/Cy0;UAS-TBPH^{N493D}/Tb x w^{1118}	0	667	**0.00**	0.25	206
GMR/Cy0;UAS-TBPH^{N493D}/Tb x UAS-dnc.RNAi	161	733	**0.22**	0.25	42
GMR/Cy0;UAS-TBPH^{N493D}/Tb x UAS-PKA-R2.RNAi	189	756	**0.25**	0.25	18
GMR/CyO;UAS-TBPH^{WT}/Tb x w.1118	1	173	**0.01**	0.25	70
GMR/CyO;UAS-TBPH^{WT}/Tb x UAS-dnc.RNAi	51	190	**0.27**	0.25	6
GMR/CyO;UAS-TBPH^{WT}/Tb x UAS-PKA-R2.RNAi	57	200	**0.29**	0.25	2
GMR/CyO x w^{1118}	246	488	**0.50**	0.50	15
GMR/CyO x UAS-dnc.RNAi	128	239	**0.54**	0.50	11
GMR/CyO x UAS-PKA-R2.RNAi	125	239	**0.52**	0.50	5

C

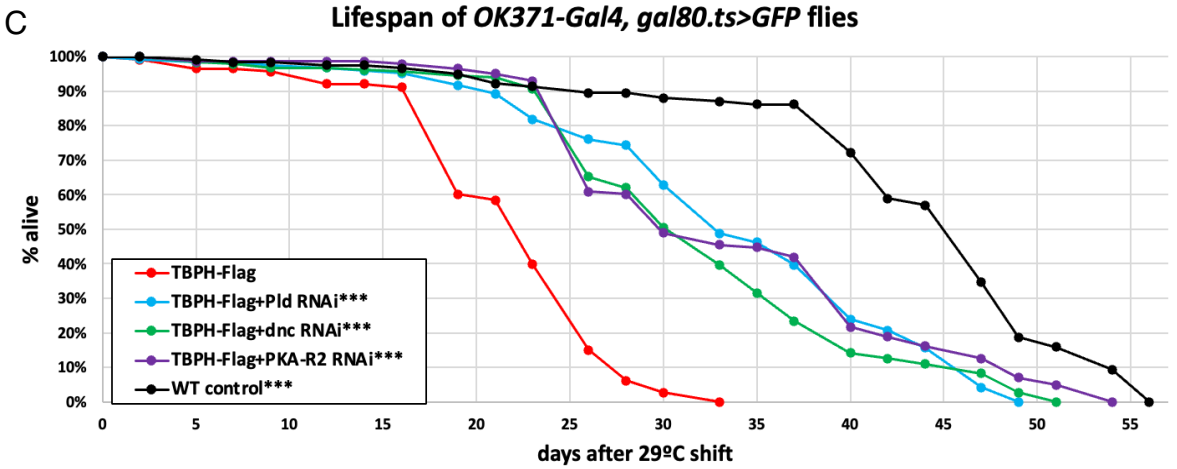

Fig. 1. Identification and validation of negative regulators of the cAMP/PKA pathway as TBPH modifiers. (*A*) *Dunce (dnc)*, a member of the cAMP/PKA signaling pathway, is both a known interactor of PA and a TDP-43/FUS modifier from our previous screen (16). An additional two cAMP/PKA pathway members, *PKA-R2* and *EPAC*, were also identified in the screen. *dnc* and *PKA-R2* (marked in red) are both negative regulators of the core PKA signaling pathway. (*B*) RNAi-based knockdown of *dnc* (*dnc^{JF02561}*) or *PKA-R2* (*PKA-R2^{JF02759}*) in the *GMR-Gal4; UAS-TBPH^{N493D}* and *GMR-Gal4; UAS-TBPH^{WT}* fly models strongly reduces TBPH-induced lethality and restores the number of progeny to near-Mendelian ratios. Some genetic components are indicated in shorthand as follows: GMR: GMR-gal4; Tb: TM6b,Tb^{1},TubP-Gal80. The number of dead non-Tb pupae is also correspondingly reduced. Note that it is impossible to distinguish CyO vs. non-CyO in pupae, but CyO does not affect lethality in adults. (*C*) An adult-onset lifespan assay in the *OK371-Gal4, UAS-mcd8-GFP; gal80.ts* background, in which transgene activation is induced by a temperature shift to 29 °C posteclosion, reveals that the TBPH-Flag-induced lifespan reduction (red line, n = 117) compared to WT control (black line, n = 120) can be significantly rescued by knockdown of *Pld* (*UAS-Pld RNAi^{HMS00529}*, blue, n = 124), *dnc* (*UAS-dnc RNAi^{JF02561}*, green, n = 188), or *PKA-R2* (*UAS-PKA-R2 RNAi^{JF02759}*, purple, n = 147). ***P < 0.001 compared to TBPH-Flag alone (log-rank test).

expressing *TBPH* alone received a score of 4, indicating the highest degree of aggregation, with the remainder receiving a score of 3. The majority of cells expressing *TBPH* along with *Pld RNAi* received a score of 3, whereas a significant proportion of both *TBPH+dnc RNAi* and *TBPH+PKA-R2 RNAi* cells scored 1 or 2 (Fig. 2*E*).

To determine the degree of aggregation using a more quantitative and unbiased method, we developed a segmentation algorithm to isolate α-TBPH-positive regions in the cytoplasm. This analysis revealed that both *TBPH+dnc RNAi* and *TBPH+PKA-R2 RNAi*-expressing cells showed a significantly greater degree of cytoplasmic TBPH coverage than cells expressing *TBPH* alone, consistent with more diffuse protein distribution (Fig. 2*F*). *Pld RNAi* did not significantly increase this parameter, reflecting the observation that TBPH protein in these cells appears to be broadly distributed among a greater number of smaller dense aggregates (Fig. 2 *B* and *F*). When we quantified the total number of discrete TBPH-positive regions in each cell, we found that *Pld RNAi* did indeed increase this parameter in a statistically significant manner, consistent with the presence of smaller and more dispersed aggregates (Fig. 2*G*). In keeping with the large number of very small puncta we observe in *dnc RNAi* and *PKA-R2 RNAi*-expressing cells, these genotypes also show a significant increase in the total number of TBPH-positive regions (Fig. 2 *C*, *D*, and *G*).

Changes in TBPH Localization. TBPH aggregation is deeply interconnected with and possibly dependent upon the mislocalization of nuclear TBPH to the cytoplasm (12). We thus asked whether modulating the Pld and PKA pathways could affect the subcellular localization of ectopic TBPH. When *UAS-TBPH^{N493D}* is expressed under the motor neuron-specific *OK371-Gal4* driver, the majority of the ectopic TBPH is cytoplasmic (Fig. 3*A*), with a mean normalized nuclear-to-cytoplasmic α-TBPH signal intensity ratio of approximately 0.8; *UAS-TBPH^{WT}* behaves in a similar manner, suggesting that the N493D mutation does not affect TBPH localization (Fig. 3 *F–H* and *SI Appendix*, Fig. S2 *C* and *D*). These measurements are consistent with qualitative observations reported in our previous study (16). Notably, unlike with the *Dip-α-Gal4* driver, we do not observe large aggregates when either TBPH allele is driven by *OK371-Gal4*, although the distribution within the cytoplasm is not homogeneous; this is likely due to lower levels of transgene

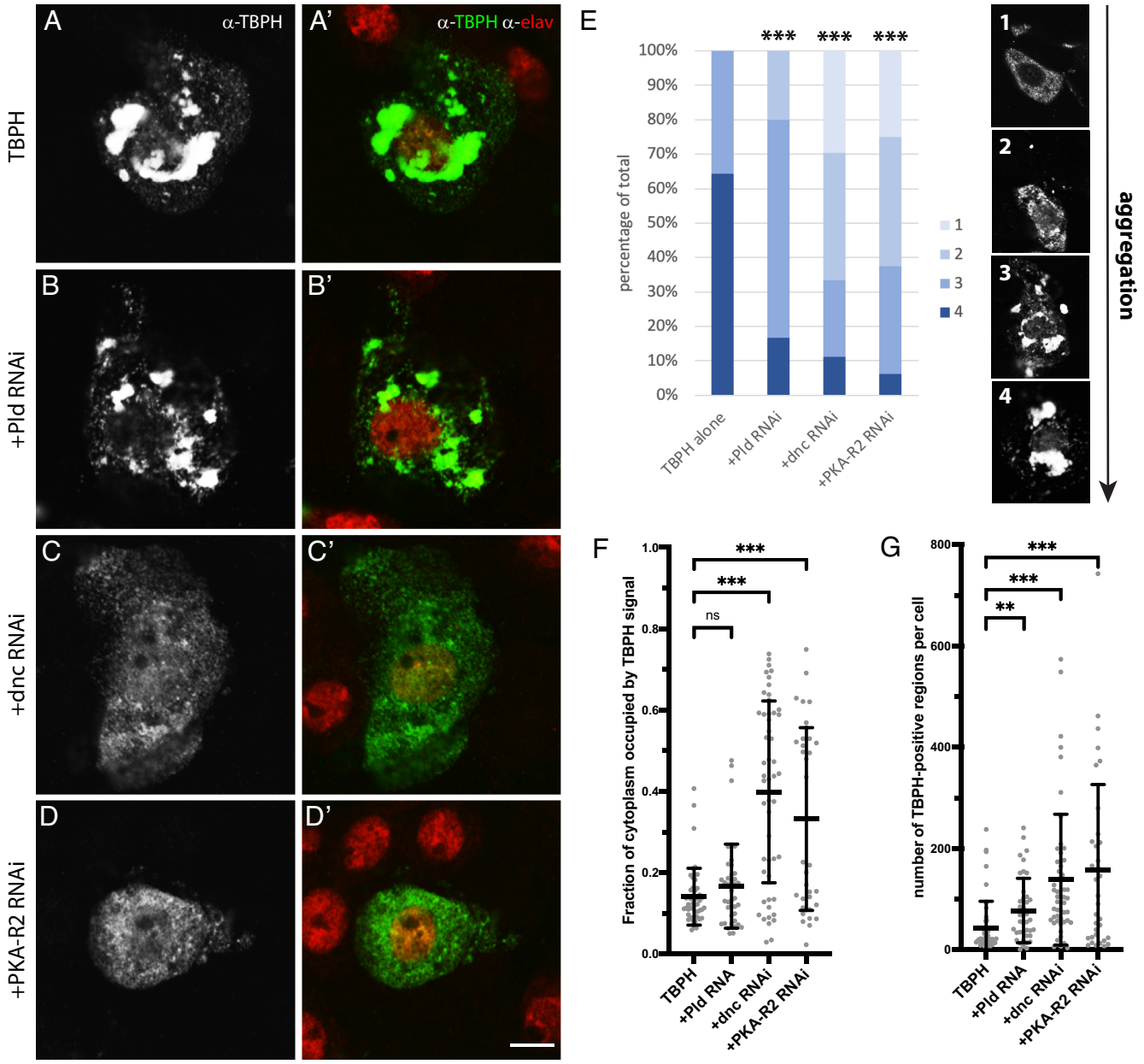

Fig. 2. Knockdown of *Pld*, *dnc*, or *PKA-R2* reduces TBPH aggregation. (*A–D'*) T3 MNISN-IS motor neurons expressing *Dip-α-Gal4; UAS-TBPH*^{WT} alone (*A, A'*) or with *UAS-Pld RNAi*^{HMS00529} (*B, B'*), *UAS-dnc RNAi*^{JF02561} (*C, C'*), or *UAS-PKA-R2 RNAi*^{JF02759} (*D, D'*) were stained for α-TBPH and α-elav. The degree of TBPH aggregation was assessed using both (*E*) qualitative [using a visual scale from least (1) to most (4) aggregated] and (*F* and *G*) quantitative [fraction of the cytoplasmic area occupied by α-TBPH signal (*F*) or number of discrete TBPH-positive regions per cell (*G*)] scales. ***$P < 0.001$, **$P < 0.01$, ns: not significant [chi-square (*E*) or student's *t* test (*F* and *G*)]. (Scale bar: 5 μ.)

activation in each individual cell. As the large aggregates make effective quantification of overall TBPH signal intensity difficult, we chose to use the *OK371-Gal4* model in order to assess localization.

Knockdown of *Pld*, *dnc*, *PKA-R1*, or *PKA-R2* results in a clearly visible nuclear shift of the TBPH^{N493D} signal (Fig. 3 *B–E*) compared to MNs expressing *TBPH*^{N493D} alone (Fig. 3*A*). The visual observations are corroborated by quantification of the α-TBPH nuclear-to-cytoplasmic ratios (Fig. 3 *F–H*). We quantified both TBPH^{N493D} and TBPH^{WT} localization and corroborated the *dnc*, *PKA-R1*, and *PKA-R2* results with second independent RNAi alleles to eliminate the possibility of off-target effects. A significant nuclear shift of α-TBPH signal was observed in every case (Fig. 3 *F–H*).

In order to distinguish between overexpressed and endogenous TBPH in this assay, we expressed a Flag-tagged wild-type TBPH in the same background and assessed the nuclear-to-cytoplasmic ratio of the α-Flag signal. We observed a significant nuclear shift of the α-Flag signal consistent with our results with α-TBPH (*SI Appendix*, Fig. S3 *A–E*). Furthermore, a Western blot from *OK371-Gal4, UAS-TBPH-Flag* larval heads reveals that TBPH-Flag levels are unaffected by *dnc RNAi*, indicating that the change in the nuclear-to-cytoplasmic ratio is unlikely to be caused by changes in protein stability or expression levels (*SI Appendix*, Fig. S3*F*).

We also determined that RNAi lines against two other hits from our screen, the ALS-associated gene *Gle1* (30) and the PA-interactor *Msp300* (20), do not affect the nuclear-to-cytoplasmic ratio of TBPH^{WT} (*SI Appendix*, Fig. S4), indicating that changes in TBPH localization are not a nonspecific effect of RNAi expression. Furthermore, these genes may affect TBPH phenotypes independent of TBPH localization.

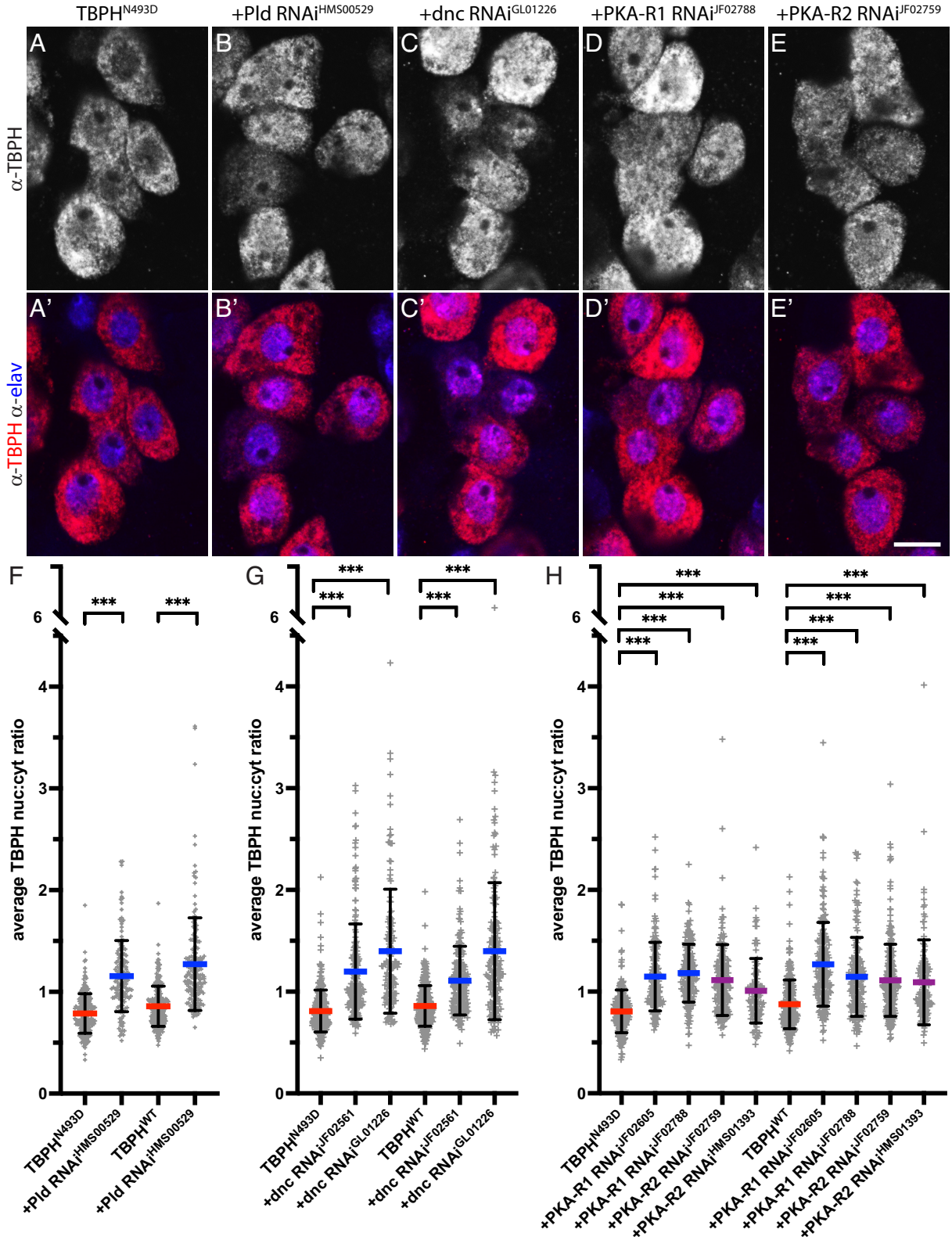

Fig. 3. Knockdown of *Pld*, *dnc*, *PKA-R1*, or *PKA-R2* causes a cytoplasmic-to-nuclear shift of TBPH. (*A–E'*) The cytoplasmic α-TBPH signal (white in *A-E*, red in *A'-E'*) in *OK371-Gal4, UAS-mcd8-GFP; UAS-TBPH*^{N493D} MNs (*A, A'*) undergoes a nuclear shift when *Pld* (*B, B'*), *dnc* (*C, C'*), *PKA-R1* (*D, D'*), or *PKA-R2* (*E, E'*) are knocked down via RNAi in T3 larval motor neuron cell bodies. Nuclei are counterstained with α-elav (blue). (Scale bar: 10 μ.) The average nuclear-to-cytoplasmic ratio of TBPH^{N493D} or TBPH^{WT} under these conditions is quantified in (*F–H*). ***$P < 0.001$ (student's *t* test). *Pld RNAi* increased the ratio from 0.79 (n = 210) to 1.16*** (n = 142) and 0.86 (n = 252) to 1.27*** (n = 167) for TBPH^{N493D} and TBPH^{WT} respectively. *dnc RNAi*^{JF02561} increased the ratios from 0.81 (n = 324) to 1.20*** (n = 202) for TBPH^{N493D} and from 0.86 (n = 321) to 1.11*** (n = 193) for TBPH^{WT}, and *dnc RNAi*^{GL01226} increased them to 1.40*** (n = 139) for TBPH^{N493D} and 1.40*** (n = 163) for TBPH^{WT}. *PKA-R1 RNAi*^{JF02605} increased the ratios from 0.81 (n = 253) to 1.15*** (n = 167) and from 0.88 (n = 304) to 1.27*** (n = 207) for TBPH^{N493D} and TBPH^{WT} respectively, while *PKA-R1 RNAi*^{JF02788} resulted in a TBPH^{N493D} ratio of 1.18*** (n = 163) and a TBPH^{WT} ratio of 1.15*** (n = 154). *PKA-R2 RNAi*^{JF02759} increased the ratio to 1.11*** (n = 172) for TBPH^{N493D} and 1.11*** (n = 268) for TBPH^{WT}, and *PKA-R2 RNAi*^{HMS01393} increased it to 1.01*** (n = 103) and 1.10*** (n = 133) respectively.

Our results clearly show that the subcellular localization of pathological TBPH is specifically sensitive to levels of *Pld*, *dnc*, *PKA-R1,* and *PKA-R2*.

Effects on Motor Function. We also evaluated the functional consequences of downregulating Pld and PKA pathway components on adult locomotor defects caused by TBPH. To that end, we utilized an adult-onset negative geotaxis assay in flies expressing *UAS-TBPH-Flag* in the temperature-sensitive *OK371-Gal4, UAS-mcd8-GFP; gal80.ts* background. Transgene expression was activated specifically in adult flies by shifting from the permissive (18 to 23 °C) to the restrictive temperature (29 °C) for *gal80.ts*, and the ability of flies to climb at least 2 cm in 10 s was assessed at 0 and 14 d timepoints after transgene induction. At 0 d, there was no significant difference in climbing ability between flies expressing *TBPH-Flag* alone, *TBPH-Flag* + *dnc RNAi*, *TBPH-Flag* + *PKA-R2 RNAi*, *PKA-R2 RNAi*, or *WT* (*GFP* alone) controls (Fig. 4*A*). [A slight increase was observed with *dnc RNAi* alone compared to WT at 0 d (90% vs. 82%, $P < 0.01$) (Fig. 4*A*); however, since this increase does not persist at 14 d (Fig. 4*B*), it is unlikely to have a significant impact on our analysis.] In contrast, at 14 d, the *TBPH-Flag* flies demonstrated severely reduced climbing ability compared to WT controls (27% vs. 57%, $P < 0.001$) (Fig. 4*B*). *dnc RNAi* and *PKA-R2 RNAi* were both able to significantly rescue this TBPH-induced climbing defect to near-wild-type levels [52% ($P < 0.001$) and 51% ($P < 0.001$) respectively] (Fig. 4*B*).

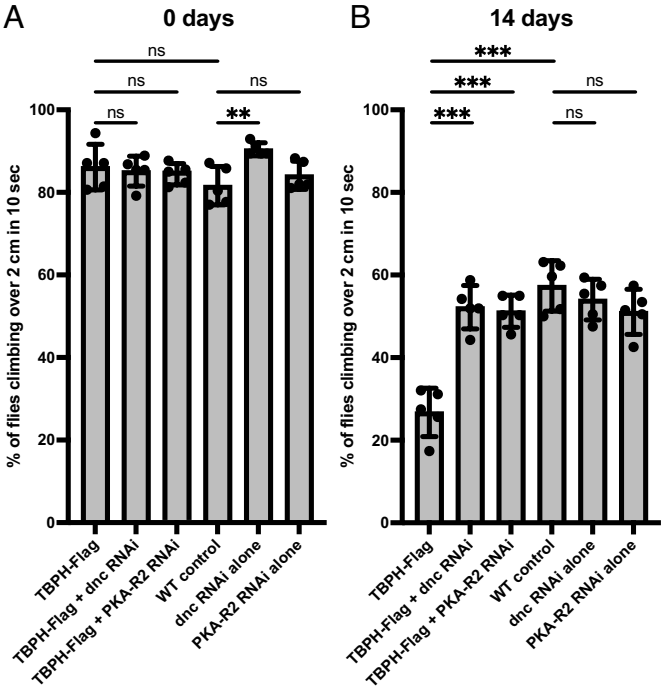

Fig. 4. Adult-onset negative geotaxis assay for *Drosophila* motor function. Flies expressing *UAS-TBPH-Flag* along with *UAS-dnc RNAi*^{JF02561} or *UAS-PKA-R2 RNAi*^{JF02759} in the temperature-conditional *OK371-Gal4, UAS-mcd8-GFP; gal80.ts* background were reared to adulthood at permissive temperature (18-23 °C, no transgene expression) and subsequently shifted to restrictive temperature (29 °C, transgene expression activated). Flies were assessed for their ability to climb a vertical distance of 2 cm within a 10 s time period at 0 d (*A*) and 14 d (*B*) after transgene activation. [n = 124 (*TBPH-Flag*, 0d), 144 (*TBPH-Flag+dnc RNAi*, 0d), 187 (*TBPH-Flag+PKA-R2* RNAi, 0 d), 148 (*WT*, 0d), 113 (*dnc RNAi*, 0d), 111 (*PKA-R2 RNAi*, 0d), 109 (*TBPH-Flag*, 14d), 131 (*TBPH-Flag+dnc RNAi*, 14d), 171 (*TBPH-Flag+PKA-R2 RNAi*, 14 d), 114 (*WT*, 14d), 101 (*dnc RNAi*, 14d), 101 (*PKA-R2 RNAi*, 14d)] $^{**}P < 0.01$, $^{***}P < 0.001$ (ANOVA).

Pld and TBPH Influence PKA Signaling Activity in TBPH-Overexpressing MNs. Our results show that knockdown of *dnc* (which results in increased PKA signaling) and knockdown of *Pld* act in the same direction to mitigate TBPH-induced phenotypes. If, as we hypothesize based on the literature, the Pld product PA directly interacts with dnc, Pld knockdown should lead to enhanced PKA signaling in TBPH models (Fig. 5*I*). In order to directly assess PKA signaling activity, we utilized a transgenic reporter, *UAS-PKA-SPARK*, in which PKA kinase activity induces the formation of bright fluorescent puncta (31, 32). The relative degree of PKA signaling is determined by counting the number of PKA-SPARK puncta in each individual cell, normalized to cell area. Expression of the *PKA-SPARK* reporter in wild-type T3 MNISN-IS motor neurons (*Dip-α-Gal4; UAS-PKA-SPARK*) reveals active PKA signaling, with 3.3 ± 1.2 PKA-SPARK puncta per arbitrary unit area (Fig. 5 *A* and *E*). The concomitant expression of *UAS-TBPH-Flag* in this background severely reduces the number of puncta by more than 75% (0.7 ± 0.6 puncta, $P < 0.001$ vs. control), indicating that TBPH-Flag itself has a strong negative impact on PKA kinase activity (Fig. 5 *C* and *E*). Knockdown of Pld partially reverses this TBPH-Flag-induced effect and more than doubles the number of puncta per unit area (1.6 ± 1.0, $P < 0.001$ vs. TBPH-Flag alone) (Fig. 5 *D* and *E*), consistent with our hypothesis that Pld acts upstream of PKA signaling in this context.

Overexpression of the PKA Target CREB Rescues TBPH Localization. The transcription factor cAMP Response Element Binding protein (CREB) is a well-characterized direct target of PKA phosphorylation that has been implicated in numerous neurogenic and neuroprotective processes in flies and mammals (24, 33, 34). Furthermore, TDP-43 overexpression can inhibit the activation and transcriptional activity of CREB in cultured rat cortical neurons (35), consistent with our observation that TBPH overexpression reduces PKA-SPARK reporter activation (Fig. 5 *C* and *E*). We therefore asked whether increasing the level of the fly CREB ortholog *CrebA* could phenocopy knockdown of *dnc* or *PKA-R2* in our TBPH localization assay. Indeed, overexpression of CrebA in *OK371-Gal4; UAS-TBPH*^{N493D} motor neurons results in a significant nuclear shift of TBPH signal (Fig. 5 *F–H*), suggesting that the PLD/PA-cAMP/PKA signaling axis can act through CREB.

Taken together, our results support a model whereby downregulation of the Pld/PA pathway causes an increase in cAMP/PKA signaling, which subsequently decreases mislocalization and aggregation of TBPH and ameliorates TBPH-induced locomotor defects and lifespan reduction (Fig. 5*I*).

Discussion

Here, we use *Drosophila* models that recapitulate crucial aspects of TDP-43 biology in vivo to identify cellular parameters that can influence pathological functions of TDP-43. Our earlier findings established the Pld pathway as an ALS phenotype modifier (16). In the current work, we now find that the Pld/PA and cAMP/PKA pathways interact to affect TDP-43-induced phenotypes, and establish a working model (Fig. 5*I*) that will serve as a guide for further analysis. A role for cAMP/PKA signals in regulating TDP-43 cellular behavior and function has not previously been reported. We show here that a reduction in levels of the negative signaling regulators *dnc*, *PKA-R1*, or *PKA-R2*, or an increase in the PKA target CrebA in our fly models significantly mitigates both molecular and functional pathologies induced by TDP-43 overexpression, suggesting that an increase in cAMP/PKA signaling may have potentially beneficial effects for ALS patients.

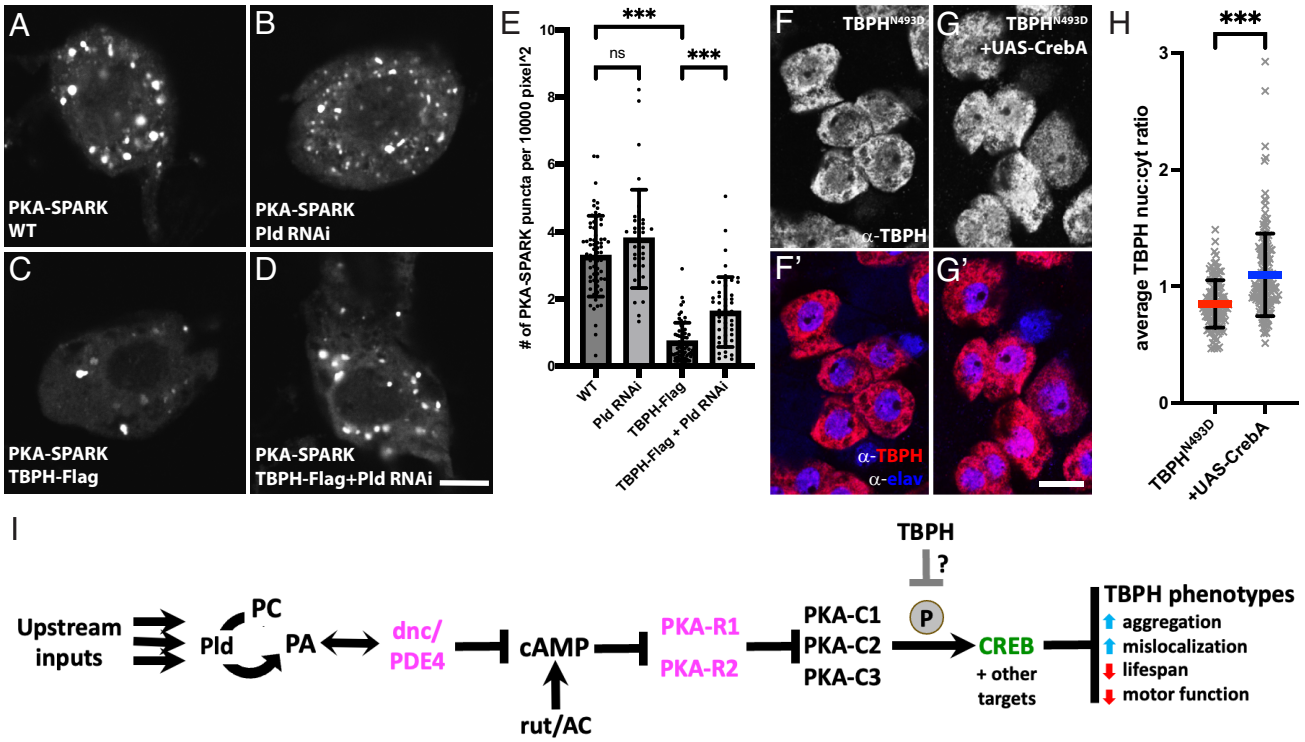

Fig. 5. PKA signaling activity is downstream of Pld and impacts TBPH localization. *Dip-α-Gal4, UAS-PKA-SPARK* flies were crossed to w^{1118} control (*A*), *UAS-Pld RNAi*^{HMS00529} (*B*), *UAS-TBPH-Flag* (*C*), or *UAS-TBPH-Flag, UAS-Pld RNAi*^{HMS00529} (*D*) lines and the native PKA-SPARK signal was imaged in MNISN-IS cells in the T3 segment of the larval VNC. Bright PKA-SPARK puncta form in the presence of active PKA signaling. [Scale bar for (*A–D*): 5 μ.] The number of PKA-SPARK puncta per cell was normalized to cell area and quantified in (*E*). Each data point shown represents the average number of puncta per 10,000 pixel^2 in a single cell. [n = 66 (*WT*), 37 (*Pld RNAi*), 62 (*TBPH-Flag*), 50 (*TBPH-Flag+Pld RNAi*)]; ***$P < 0.001$ (ANOVA). (*F-G'*) TBPH localization was visualized in *OK371-Gal4, UAS-mcd8-GFP; UAS-TBPH*^{N493D} MNs alone (*F, F'*) or with *UAS-CrebA* (*G, G'*) by immunofluorescence staining for α-TBPH and α-elav. [Scale bar for (*F* and *G*): 10 μ.] (*H*) The average nuclear-to-cytoplasmic ratio of TBPH shifts from 0.85 (n = 121) for *TBPH*^{N493D} alone to 1.10 (n = 161) for *TBPH*^{N493D} + *CrebA* [***$P < 0.001$ (student's *t* test)]. (*I*) Working model for how the Pld/PA and cAMP/PKA pathways interact to affect various TBPH-induced phenotypes. Negative PKA signaling regulators (*dnc*, *PKA-R1, PKA-R2*) tested in the current study are labeled in magenta, and positive regulators (*CREB*) in green.

The involvement of TDP-43 in ALS pathology is by now a well-documented fact. In addition to the relatively small proportion of patients in whom mutations in the TDP-43 gene itself cause inherited forms of ALS, nearly all cases, whether they be familial or sporadic, display TDP-43 aggregate pathology (11). This ubiquity has led to the broad assumption that aggregates may be critical, if not causative, for disease progression, but the cellular and genetic factors affecting aggregation still remain largely unknown. Moreover, by the time aggregates are observed, it may be too late for successful therapeutic intervention.

Pathologic manifestation of ALS is also marked by the mislocalization of TDP-43 protein from the nucleus to the cytoplasm, which may represent an earlier and more reversible step in disease progression (12). Although the mechanisms by which TDP-43 mislocalization and aggregation influence one another are not well understood, the data we present here supports the notion that these two critical processes are coregulated by cAMP/PKA. Whether or not preexisting mislocalization and/or aggregation can be reversed in the presence of increased cAMP/PKA signaling remains an open question. The *Drosophila* model, with its genetic tractability and multiple, independently controlled gene expression systems, may have much to offer in this context, as conditional, independent expression of *TBPH* and interacting factors such as *dnc* and *PKA-R2* will allow us to explore the kinetics of in vivo mislocalization and aggregation in a systematic manner.

We show that PKA exerts its effect on TDP-43 at least partially through the transcription factor CREB (Fig. 5). The work of Herzog et al. showing that TDP-43 dysfunction results in impaired CREB signaling and, consequently, dendritic branching defects in cultured rat cortical neurons also lends support to this finding (35). However, given that PKA phosphorylates many substrates in addition to CREB, we cannot rule out the possibility that other PKA targets may play a role in TDP-43 regulation. Indeed, PKA was shown to be able to phosphorylate TDP-43 directly in one in vitro study, although the biological significance of this observation remains unclear (36). Our results also suggest that TDP-43 activity itself can inhibit PKA signaling (Fig. 5), pointing to the intriguing possibility of a feedback loop mechanism in which TDP-43 overexpression amplifies its own deleterious effects by bypassing PKA-driven regulatory control.

Although the PKA pathway is the most well-studied target of cAMP, it is important to note that cAMP has other known effectors, namely the cyclic nucleotide gated ion channels and the guanine nucleotide exchange factor *EPAC* (33). Notably, *EPAC* was also identified in our screens as a TDP-43/FUS modifier (Fig. 1) (16). Although our findings with PKA-R2 and CREB point to a definitive role of the PKA branch of the cAMP pathway in TDP-43 biology, it would not be surprising if EPAC is also involved. Of particular interest, given the importance of TDP-43 subcellular localization to ALS pathology, is a report that EPAC and PKA can act in opposition to one another to maintain the nuclear-cytoplasmic balance of the DNA-PK protein (37).

Although cytoplasmic mislocalization and aggregation of TDP-43 unquestionably causes toxic gain-of-function effects, it has also been linked to a loss of physiological TDP-43, which acts in healthy cells to regulate RNA processing, gene transcription, and protein

homeostasis (10, 17). Along these lines, both loss- and gain-of-function models in rodents and flies demonstrate ALS-like phenotypes, and it is likely that both perturbations, possibly simultaneously, have their role to play in disease progression (14, 17). Thus, it will be important to determine whether cAMP/PKA pathway activation impacts the normal physiological functions of TDP-43 such as splicing, RNA binding, and transcriptional regulation.

Interestingly, several studies have shown decreased levels of CREB-dependent transcription in brains from AD patients and mouse models, which may be responsible for β-amyloid-induced synaptic and cognitive defects (34, 38). Pld has likewise been implicated in AD (39–41). Given the growing body of evidence that a significant proportion of AD cases may also fall under the broad class of TDP-43 proteinopathies (9, 11), the link between PKA/CREB and TDP-43 may be worth pursuing in AD as well as ALS.

Notably, the RNAi reagents we used in this study are unlikely to result in complete elimination of gene function (42). This is encouraging, as it suggests that partial pharmacological inhibition of dnc/PDE4 or PKA-R2 function or, conversely, a modest activation of cAMP/PKA pathway activity, may be sufficient to convey therapeutic benefits without the severe side effects associated with total loss of gene function. To that end, the PKA pathway has long been considered a promising therapeutic target. In particular, there are several decades-worth of preclinical and clinical studies on a wide range of PDE4 inhibitors, not only for neurological disorders including AD, but also for conditions as diverse as respiratory diseases, psoriasis, and autoimmune disorders (43–45). However, the relatively poor efficacy and severe side effects of many of these compounds have allowed only a small number to be approved for use as drugs in recent years (43, 44). No PDE4-specific inhibitors have been tested against ALS to date, although Ibudilast, a nonselective phosphodiesterase inhibitor (among other targets), is currently undergoing clinical trials for ALS (46). Our data suggest that selective inhibitors of dnc/PDE4 may hold promise for ALS therapeutic intervention.

Materials and Methods

Fly Strains. All fly strains were maintained at 18 °C or 25 °C on standard *Drosophila* media. Crosses were performed at 25 °C unless otherwise noted. The following fly strains were used: w^{1118}, *OK371-Gal4* [Bloomington *Drosophila* Stock Center (BDSC) #26160], *Dip-α-Gal4* (BDSC #90319), *GMR-Gal4* (BDSC #1104), $gal80^{ts}$ (BDSC #7108), *UAS-TBPH*^{WT} (16), *UAS-TBPH*^{N493D} (16), *UAS-TBPH-Flag* (BDSC #93601), *UAS-PKA-SPARK* (32), and *UAS-CrebA* (BDSC #79021). RNAi lines used were *UAS-Pld RNAi*^{HMS00529} (BDSC #32839), *UAS-dnc RNAi*^{JF02561} (BDSC #27250), *UAS-dnc RNAi*^{GL01266} (BDSC #41644), *UAS-PKA-R1 RNAi*^{JF02605} (BDSC #27308), *UAS-PKA-R1 RNAi*^{JF02788} (BDSC #27708), *UAS-PKA-R2 RNAi*^{JF02759} (BDSC #27680), *UAS-PKA-R2 RNAi*^{HMS01393} (BDSC #34983), UAS-Gle1 RNAi^{HMC03626} (BDSC #52888), and UAS-Msp300 RNAi^{HMC03198} (BDSC #51460).

GMR-Gal4 Assays. The retinal degeneration assay was performed as described in our previous work (16). The toxicity assay was performed by crossing *GMR-Gal4/CyO; UAS-TBPH/TM6b,Tb*^{1},*TubP-Gal80,* or *GMR-Gal4/CyO* (for RNAi only controls) virgin females with *UAS-RNAi* lines of interest. The number of viable adult progeny of each genotype, including all balancer genotypes, was counted at 16 to 17 d after cross initiation, as were dead (black) non-Tb pupae.

Lifespan Assay. For TBPH-Flag lifespan assays, *OK371-Gal4, UAS-mcd8-GFP; gal80.ts* virgin females were crossed to males bearing various combinations of *UAS-TBPH-Flag* and *UAS-RNAi* alleles. For hTDP-43^{M337V} lifespan assays, *OK6-Gal4, gal80.ts; UAS-hTDP43*^{M337V} virgins were crossed to *UAS-RNAi* males. Crosses were reared until adulthood at 18 to 23 °C, to allow for gal80-induced repression of transgene expression (28). Adult female progeny were collected within 7 d after eclosion and shifted to 29 °C to inactivate gal80 and thus activate transgene expression. The day on which flies are shifted to 29 °C is Day 0 in the assays. Live flies were subsequently flipped and counted every 2 to 3 d. Lifespan analysis was performed using the OASIS2 platform [https://sbi.postech.ac.kr/oasis2/ (47).

Immunofluorescence Staining. Late third instar larvae were partially dissected in 1X PBS and fixed in 1X PBS + 4% paraformaldehyde for 20 min at room temperature (RT), followed by permeabilization and blocking in blocking solution (1X PBS + 0.1% Triton X-100 + 5 mg/mL BSA) at RT. Samples were incubated for at least 16 h at 4 °C with primary antibody in blocking solution, followed by washing and incubation in secondary antibody in blocking solution for 2.5 h at RT. Larval brains were isolated after staining and mounted in Vectashield Plus with DAPI (Vector Labs #H-2000), with the dorsal surface facing up.

The guinea pig α-TBPH polyclonal antibody was generated and purified for us by Genscript and used at a concentration of 1:500. Rat α-elav (Developmental Studies Hybridoma Bank #7E8A10) was used at 1:100. α-Flag-M2 (Sigma-Aldrich #F3165) was used at 1:2,000. α-guinea pig-AlexaFluor647 (Invitrogen #A21450) and α-rat-AlexaFluor568 (Invitrogen #A11077) secondary antibodies were used at 1:1,000.

Imaging was performed on a Nikon Ti2 microscope with AX R point-scanning confocal and a Nikon Ti microscope with A1R point scanning confocal at the Nikon Imaging Center at Harvard Medical School. All images were acquired with a 60× objective lens. Images were analyzed using FIJI/ImageJ. Brightness and contrast were adjusted for publication (identically for all images in a single dataset) using Adobe Photoshop.

TBPH Aggregation Analysis. All aggregation experiments were performed in late third instar female *Dip-α-Gal4* larvae stained for α-TBPH along with α-elav. In some cases, an additional nuclear marker (α-lamin Dm0) was also stained. Individual images were analyzed using three input components in the α-TBPH channel: a raw input image, a cell mask, and a nucleus mask. To pinpoint the cell of interest within the image, we manually marked the corresponding cell and nucleus masks. The TBPH aggregates were then segmented from the raw image using the Otsu thresholding method, which facilitates binary segmentation between the background and the foreground aggregates. Subsequently, various metrics were computed by combining information from the raw image, segmented image, cell mask, and nucleus mask. The quantification of TBPH aggregates focused on the cytoplasmic region of the cell, obtained by subtracting the nucleus mask from the cell mask. TBPH aggregate area and number were computed by tallying the foreground pixels within the segmented image that fall within the cytoplasmic region.

Quantification of TBPH Nuclear:Cytoplasmic (N:C) Ratios. All N:C ratio experiments were performed on late third instar larvae reared at 18 °C. We imaged and analyzed the 10 stereotypical dorsomedial MN cell bodies in the T3 segment (48). Cell boundaries were determined by native mcd8-GFP fluorescence and nuclei by α-elav staining. The average intensity of α-TBPH signal (labeled with AlexaFluor 647) in nuclei and whole cells, normalized to area, was quantified using FIJI, and the data were further analyzed using Microsoft Excel and GraphPad Prism.

Western Blotting. Late third instar larval heads were dissected in PBS and homogenized in lysis buffer containing 1% NP-40 and 1% Triton X-100. Primary antibodies used for western blotting were α-TBPH (see above), α-FlagM2 (Sigma-Aldrich #A8592), and E7 α-beta-tubulin (Developmental Studies Hybridoma Bank #E7).

Negative Geotaxis (Climbing) Assay. Crosses and conditions for climbing assays are the same as for lifespan assays (see above). Climbing assays were performed with female flies as previously described (49) with up to 15 flies per vial. For each vial, the assay was repeated five times, and the number of flies able to climb past a distance of 2 cm in 10 s averaged over these replicates.

PKA-SPARK reporter experiments. PKA-SPARK quantitation experiments were performed by imaging native PKA-SPARK fluorescence in MNISN-Is MNs in the T3 segment of fixed VNCs from late third instar female larvae, followed by quantification of the number of PKA-SPARK puncta normalized to cell area using FIJI. Imaging and analysis conditions were identical for all samples.

Data, Materials, and Software Availability. All study data are included in this article and/or *SI Appendix*.

ACKNOWLEDGMENTS. We thank Dr. Xiaokun Shu (UCSF) for *UAS-PKA-SPARK* flies, the Bloomington Drosophila Stock Center for additional fly stocks, the Developmental Studies Hybridoma Bank for α-elav antibody, the Nikon Imaging Center at Harvard Medical School for assistance with confocal microscopy, Dr. Sarah Hernandez for assistance with climbing assays, and the members of the Artavanis-Tsakonas and Van Vactor labs for many illuminating discussions regarding this project. This study was funded by NIH R21 NS123207.

Author affiliations: [a]Department of Cell Biology, Harvard Medical School, Boston, MA 02115; [b]Department of Pathology, Brigham and Women's Hospital, Harvard Medical School, Boston, MA 02115; [c]Department of Pathology, Massachusetts General Hospital, Harvard Medical School, Boston, MA 02114; [d]Cancer Data Science Program, Dana-Farber Cancer Institute, Boston, MA 02115; and [e]Cancer Program, Broad Institute of Harvard and MIT, Cambridge, MA 02142

Author contributions: D.M.H., D.V.V., and S.A.-T. designed research; D.M.H., M.S., F.M., P.G., and L.T. performed research; D.M.H. and M.S. contributed new reagents/analytic tools; D.M.H., M.S., D.V.V., and S.A.-T. analyzed data; and D.M.H., D.V.V., and S.A.-T. wrote the paper.

1. M. C. Kiernan *et al.*, Amyotrophic lateral sclerosis. *Lancet* **377**, 942–955 (2011).
2. G. Lin, D. Mao, H. J. Bellen, Amyotrophic lateral sclerosis pathogenesis converges on defects in protein homeostasis associated with TDP-43 mislocalization and proteasome-mediated degradation overload. *Curr. Top. Dev. Biol.* **121**, 111–171 (2017).
3. E. Buratti, Functional significance of TDP-43 mutations in disease. *Adv. Genet.* **91**, 1–53 (2015).
4. E. Kabashi *et al.*, TARDBP mutations in individuals with sporadic and familial amyotrophic lateral sclerosis. *Nat. Genet.* **40**, 572–574 (2008).
5. J. Sreedharan *et al.*, TDP-43 mutations in familial and sporadic amyotrophic lateral sclerosis. *Science* **319**, 1668–1672 (2008).
6. J. Cooper-Knock *et al.*, Advances in the genetic classification of amyotrophic lateral sclerosis. *Curr. Opin. Neurol.* **34**, 756–764 (2021).
7. D. M. Wilson III *et al.*, Hallmarks of neurodegenerative diseases. *Cell* **186**, 693–714 (2023).
8. M. Neumann *et al.*, Ubiquitinated TDP-43 in frontotemporal lobar degeneration and amyotrophic lateral sclerosis. *Science* **314**, 130–133 (2006).
9. A. Prasad, V. Bharathi, V. Sivalingam, A. Girdhar, B. K. Patel, Molecular mechanisms of TDP-43 misfolding and pathology in amyotrophic lateral sclerosis. *Front. Mol. Neurosci.* **12**, 25 (2019).
10. T. R. Suk, M. W. C. Rousseaux, The role of TDP-43 mislocalization in amyotrophic lateral sclerosis. *Mol. Neurodegener.* **15**, 45 (2020).
11. M. Jo *et al.*, The role of TDP-43 propagation in neurodegenerative diseases: Integrating insights from clinical and experimental studies. *Exp. Mol. Med.* **52**, 1652–1662 (2020).
12. P. Tziortzouda, L. Van Den Bosch, F. Hirth, Triad of TDP43 control in neurodegeneration: Autoregulation, localization and aggregation. *Nat. Rev. Neurosci.* **22**, 197–208 (2021).
13. L. McGurk, A. Berson, N. M. Bonini, Drosophila as an in vivo model for human neurodegenerative disease. *Genetics* **201**, 377–402 (2015).
14. D. C. Diaper *et al.*, Loss and gain of Drosophila TDP-43 impair synaptic efficacy and motor control leading to age-related neurodegeneration by loss-of-function phenotypes. *Hum. Mol. Genet.* **22**, 1539–1557 (2013).
15. H. J. Kim *et al.*, Therapeutic modulation of eIF2alpha phosphorylation rescues TDP-43 toxicity in amyotrophic lateral sclerosis disease models. *Nat. Genet.* **46**, 152–160 (2014).
16. M. W. Kankel *et al.*, Amyotrophic lateral sclerosis modifiers in Drosophila reveal the phospholipase D pathway as a potential therapeutic target. *Genetics* **215**, 747–766 (2020).
17. E. N. Guerrero *et al.*, TDP-43/FUS in motor neuron disease: Complexity and challenges. *Prog. Neurobiol.* **145–146**, 78–97 (2016).
18. H. A. Brown, P. G. Thomas, C. W. Lindsley, Targeting phospholipase D in cancer, infection and neurodegenerative disorders. *Nat. Rev. Drug Discov.* **16**, 351–367 (2017).
19. R. Thakur, A. Naik, A. Panda, P. Raghu, Regulation of membrane turnover by phosphatidic acid: Cellular functions and disease implications. *Front. Cell Dev. Biol.* **7**, 83 (2019).
20. J. H. Jang, C. S. Lee, D. Hwang, S. H. Ryu, Understanding of the roles of phospholipase D and phosphatidic acid through their binding partners. *Prog. Lipid Res.* **51**, 71–81 (2012).
21. M. Grange *et al.*, The cAMP-specific phosphodiesterase PDE4D3 is regulated by phosphatidic acid binding. Consequences for cAMP signaling pathway and characterization of a phosphatidic acid binding site. *J. Biol. Chem.* **275**, 33379–33387 (2000).
22. E. Huston, I. Gall, T. M. Houslay, M. D. Houslay, Helix-1 of the cAMP-specific phosphodiesterase PDE4A1 regulates its phospholipase-D-dependent redistribution in response to release of Ca2+. *J. Cell Sci.* **119**, 3799–3810 (2006).
23. N. Gervasi, P. Tchenio, T. Preat, PKA dynamics in a Drosophila learning center: Coincidence detection by rutabaga adenylyl cyclase and spatial regulation by dunce phosphodiesterase. *Neuron* **65**, 516–529 (2010).
24. D. Lee, Global and local missions of cAMP signaling in neural plasticity, learning, and memory. *Front. Pharmacol.* **6**, 161 (2015).
25. L. Scheunemann, P. Y. Placais, Y. Dromard, M. Schwarzel, T. Preat, Dunce phosphodiesterase acts as a checkpoint for Drosophila long-term memory in a pair of serotonergic neurons. *Neuron* **98**, 350–365.e5 (2018).
26. F. Vonhoff, H. Keshishian, Cyclic nucleotide signaling is required during synaptic refinement at the Drosophila neuromuscular junction. *Dev. Neurobiol.* **77**, 39–60 (2017).
27. S. K. Park, S. A. Sedore, C. Cronmiller, J. Hirsh, Type II cAMP-dependent protein kinase-deficient Drosophila are viable but show developmental, circadian, and drug response phenotypes. *J. Biol. Chem.* **275**, 20588–20596 (2000).
28. S. E. McGuire, P. T. Le, A. J. Osborn, K. Matsumoto, R. L. Davis, Spatiotemporal rescue of memory dysfunction in Drosophila. *Science* **302**, 1765–1768 (2003).
29. J. Ashley *et al.*, Transsynaptic interactions between IgSF proteins DIP-alpha and Dpr10 are required for motor neuron targeting specificity. *Elife* **8**, e42690 (2019).
30. H. M. Kaneb *et al.*, Deleterious mutations in the essential mRNA metabolism factor, hGle1, in amyotrophic lateral sclerosis. *Hum. Mol. Genet.* **24**, 1363–1373 (2015).
31. J. C. Sears, K. Broadie, Temporally and spatially localized PKA activity within learning and memory circuitry regulated by network feedback. *eNeuro* **9**, ENEURO.0450-21.2022 (2022).
32. Q. Zhang *et al.*, Visualizing dynamics of cell signaling in vivo with a phase separation-based kinase reporter. *Mol. Cell* **69**, 334–346.e4 (2018).
33. P. Sassone-Corsi, The cyclic AMP pathway. *Cold Spring Harb. Perspect. Biol.* **4**, a011148 (2012).
34. C. A. Saura, J. Valero, The role of CREB signaling in Alzheimer's disease and other cognitive disorders. *Rev. Neurosci.* **22**, 153–169 (2011).
35. J. J. Herzog *et al.*, TDP-43 dysfunction restricts dendritic complexity by inhibiting CREB activation and altering gene expression. *Proc. Natl. Acad. Sci. U.S.A.* **117**, 11760–11769 (2020).
36. J. Gu, D. Chu, N. Jin, F. Chen, F. Liu, Cyclic AMP-dependent protein kinase phosphorylates TDP-43 and modulates its function in Tau mRNA processing. *J. Alzheimers Dis.* **70**, 1093–1102 (2019).
37. E. Huston *et al.*, EPAC and PKA allow cAMP dual control over DNA-PK nuclear translocation. *Proc. Natl. Acad. Sci. U.S.A.* **105**, 12791–12796 (2008).
38. M. A. R. Chowdhury, J. An, S. Jeong, The pleiotropic face of CREB family transcription factors. *Mol. Cells* **46**, 399–413 (2023).
39. D. Cai *et al.*, Phospholipase D1 corrects impaired betaAPP trafficking and neurite outgrowth in familial Alzheimer's disease-linked presenilin-1 mutant neurons. *Proc. Natl. Acad. Sci. U.S.A.* **103**, 1936–1940 (2006).
40. J. K. Jin *et al.*, Phospholipase D1 is associated with amyloid precursor protein in Alzheimer's disease. *Neurobiol. Aging* **28**, 1015–1027 (2007).
41. T. G. Oliveira *et al.*, Phospholipase d2 ablation ameliorates Alzheimer's disease-linked synaptic dysfunction and cognitive deficits. *J. Neurosci.* **30**, 16419–16428 (2010).
42. L. A. Perkins *et al.*, The transgenic RNAi project at Harvard medical school: Resources and validation. *Genetics* **201**, 843–852 (2015).
43. L. Crocetti, G. Floresta, A. Cilibrizzi, M. P. Giovannoni, An overview of PDE4 inhibitors in clinical trials: 2010 to early 2022. *Molecules* **27**, 4964 (2022).
44. J. Jin, F. Mazzacuva, L. Crocetti, M. P. Giovannoni, A. Cilibrizzi, PDE4 inhibitors: Profiling hits through the multitude of structural classes. *Int. J. Mol. Sci.* **24**, 11518 (2023).
45. A. J. Tibbo, G. S. Tejeda, G. S. Baillie, Understanding PDE4's function in Alzheimer's disease; a target for novel therapeutic approaches. *Biochem. Soc. Trans.* **47**, 1557–1565 (2019).
46. B. Oskarsson *et al.*, MN-166 (ibudilast) in amyotrophic lateral sclerosis in a Phase IIb/III study: COMBAT-ALS study design. *Neurodegener. Dis. Manag.* **11**, 431–443 (2021).
47. S. K. Han *et al.*, OASIS 2: Online application for survival analysis 2 with features for the analysis of maximal lifespan and healthspan in aging research. *Oncotarget* **7**, 56147–56152 (2016).
48. J. C. Choi, D. Park, L. C. Griffith, Electrophysiological and morphological characterization of identified motor neurons in the Drosophila third instar larva central nervous system. *J. Neurophysiol.* **91**, 2353–2365 (2004).
49. S. J. Hernandez *et al.*, An altered extracellular matrix–integrin interface contributes to Huntington's disease-associated CNS dysfunction in glial and vascular cells. *Hum. Mol. Genet.* **32**, 1483–1496 (2023).